Transaction of the Korean Society of Mechanical Engineers, Vol. 9, No. 5, pp. 663~676, 1985.

<Original>

Natural Convection in a Horizontal Cylindrical Annulus Enclosing Heat Generating Core

Keun-Shik Chang* and Se-Yoon Oh**

(Received May 21, 1985)

發熱核 주위의 수평圓環에서의 자연대류

장 근 식·오 세 윤

Key Words: Natural Convections(自然對流), Multiple Concentric Thermal Layers(多重同心熱層), Heat Generating Core(發熱核), Finite Difference Method(有限差分法), Iterative Numerical Procedure(反復數値計算)

초 록

수평원통형의 복합유동층에서의 층류자연대류를 수치적으로 연구하였다. 外側의 同心圓環이 內側의 發熱유체로 형성된 원통형 核을 둘러싸고, 그 사이에 두께가 유한하거나 두께를 무시할 수 있는 간막이 벽이 존재한다. 유동특성과 열전달에 관한 매개변수적 고찰을 시행하여 직경비, Prandtl수, 發熱强度에 기준을 둔 Rayleigh수 등의 영향을 이해하게 되었다. 간막이 벽의 두께나 열전도의 효과도 제한된 범위 안에서 고려하였다.

Nomenclature

A_0 : Heat generated by heat sources per unit time and per unit volume
C_P : Specific heat at constant pressure
$\underline{g}$: Gravitational acceleration vector
K : Thermal conductivity
L : A characteristic length, taken here as the gap size($=r_0-r_i$)
P : Pressure
Pr : Prendtl number
Ra_L : Rayleigh number, see Eq.(9)
r : Nondimensional distance, see Eq.(4)
(r, θ) : Cylindrical coordinate
T : Tempeature
T_0 : Reference temperature, that of the outer cylinder
t : Time
$\underline{u}$: Velocity vector having component(V_r, V_θ)
α : Thermal diffusivity
β : Thermal expansion coefficient
ζ : Vorticity component in the problem plane $\left(\frac{\partial V_\theta}{\partial r}+\frac{V_\theta}{r}-\frac{1}{r}\frac{\partial V_r}{\partial \theta}\right)$
ν : Kinematic viscosity
ρ : Density
ϕ : Nondimensional temperature, see Eq.(4)
Ψ : Stream function, see Eq.(5)
$\underline{\omega}$: Vorticity vector

Superscript

$*$: Refers to the dimensional quantity

Subscript

* Member, Department of Mechanical Engineering, Korea Advanced Institute of Science and Technology
**Hyundai Engineering and Construction Co., Ltd.

o : Refers to the outer cylinder
i : Refers to the inner cylinder
w : Refers to the inner cylinder wall

1. Introduction

Natural convection in horizontal annuli has been investigated for decades theoretically and experimentally. Kuehn and Goldstein[1] introduce extensive literature on this subject, where a variety of methods such as smoke-flow visualization, Mach-Zehnder interferometry and computational techniques are described.

Recently, the laminar analysis on the concentric annli has been extended to the turbulent regime by Farouk and Guceri[2] for Rayleigh numbers from 10^6 to 10^7, by using two-equation turbulence model. Other kind of extension is also made by Cho,Chang and Park[3], who studied the eccentricity effect in the horizontal annuli using computational methods in the bipolar coordinate system.

Contrary to the constant wall temperature usually assumed in the previous research, Huetz and Petit[4] considered the case of constant heat flux on one wall, while the other wall remaining isothermal. Van De Sande and Hamer[5] investigated experimentally the heat flux-driven flow in cylindrical annuli. Rotem[6] studied the free convective interaction between a solid core, which is heat dissipating as well as heat conducting, and a fluid layer in the cylindrical annular gap by expanding the stream function and the temperature in terms of the Grashof number and the Rayleigh number, respectively.

There has been relatively few studies on the natural convection by heat source distributed in one of the fluid layers under interaction, despite its many applications in the nuclear and mechanical engineering. The problem studied in the reference[7] was heat generating fluid contained in the vertical cylinders and spheres with isothermal wall conditions.

The steady state solutions were numerically obtained and an experiment was also carried by using the radioactive tritium gas for comparison purpose. For reacting gases in a horizontal cylinder, Jones[8] used A.D.I. method to investigate the natural convection due to the exothermicity of the gas, where the reaction rate of the heat sources follows Arrhenius's law for temperature dependence.

In the present paper, we studied the laminar natural convection in a concentric multi-layer composite system, the outer annular flow and the inner core with partition inbetween. The inner core fluid is assumed heat generating and the outer surface of the annulus is kept isothermal. Difficulty of the problem lies in the fact that the thermal system consists of multiple layers of fluid and solid when the partitioning wall has finite thickness, and that the thermal conditions at the interface of these layers are unknown *a priori*. In particular, when the partitioning wall has negligible thickness, the problem is reduced to a two-layer flow system. Parametric effects of the Rayleigh number, Prandtl number and the diameter ratio on the flow characteristics in the annulus are presented in the subsequent sections.

2. Governing Equations

An infinitely long horizontal cylindrical concentric annulus is filled with a Newtonian fluid The outer cylinder wall of the annulus($r=r_0$) is held at a uniform temperature, and the partitioning wall($r=r_i$ and $r=R$) is subject to heat flux whose local intensities are not known *a priori*. The fluid in the cylindrical core is assumed to have the same transport properties as that in the annulus except that it is heat

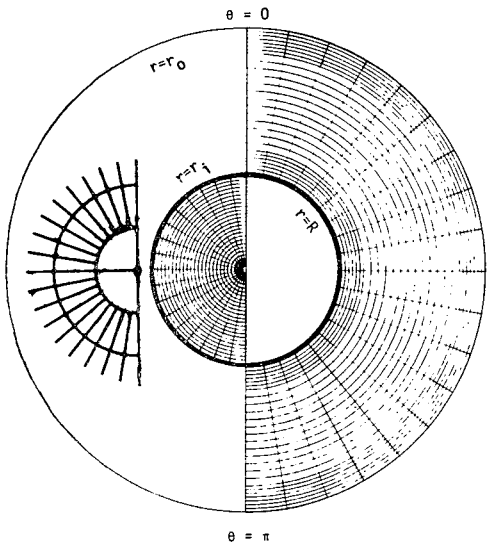

Fig. 1 Grid system for the composite layer

generating uniformly. The system is symmetrical with respect to a vertical axis passing through the center, and the variable grid is shown in Fig. 1.

2.1. Fluid Media

The steady Boussinesq Equations in dimensional form are

$$\nabla\cdot\underline{u}^*=0 \tag{1}$$

$$\frac{D\underline{u}^*}{Dt}=-\frac{1}{\rho}\nabla P^*+\nu\nabla^2\underline{u}^*+\beta(T^*-T_0^*)\underline{g} \tag{2}$$

$$\rho C_p\frac{DT^*}{Dt^*}=K\nabla^2T^*+mA_0 \tag{3}$$

where A_0 represents the heat generated per unit volume and per unit time, which is a constant. The same equations apply to both the annulus and the core, except that m=0 for the annulus and m=1 for the cylindrical core.

Introduce the following dimensionless quantities

$$\text{length}\quad r=\frac{r^*}{L}$$

$$\text{velocity (vector)}\quad \underline{u}=\frac{\underline{u}^*}{\alpha/L}$$

$$\text{temperature}\quad \phi=\frac{T^*-T_0^*}{A_0L^2/K} \tag{4}$$

$$\text{vorticity (vector)}\quad \underline{\omega}=\frac{\underline{\omega}^*}{\alpha/L^2}$$

We define the stream function

$$V_r=\frac{1}{r}\frac{\partial\Psi}{\partial\theta},\quad V_\theta=-\frac{\partial\Psi}{\partial r} \tag{5}$$

The nondimensional form of the governing equations are in the cylindrical coordinates

$$\frac{\partial^2\zeta}{\partial r^2}+\frac{1}{r}\frac{\partial\zeta}{\partial r}+\frac{1}{r^2}\frac{\partial^2\zeta}{\partial\theta^2}=\frac{1}{Pr}\left(V_r\frac{\partial\zeta}{\partial r}+\frac{V_\theta}{r}\frac{\partial\zeta}{\partial\theta}\right)+Ra_L\left(\sin\theta\frac{\partial\phi}{\partial r}+\frac{\cos\theta}{r}\frac{\partial\phi}{\partial\theta}\right) \tag{6}$$

$$\frac{\partial^2\Psi}{\partial r^2}+\frac{1}{r}\frac{\partial\Psi}{\partial r}+\frac{1}{r^2}\frac{\partial^2\Psi}{\partial^2\theta}=-\zeta \tag{7}$$

$$\frac{\partial^2\phi}{\partial r^2}+\frac{1}{r}\frac{\partial\phi}{\partial r}+\frac{1}{r^2}\frac{\partial^2\phi}{\partial\theta^2}=V_r\frac{\partial\phi}{\partial r}+\frac{V_\theta}{r}\frac{\partial\phi}{\partial\theta}-m \tag{8}$$

where ζ is the non-zero vorticity component in the plane of the problem under consideration. The Rayleigh number is defined based on the source strength A_0 and the annulus gap size L:

$$Ra_L=\frac{g\beta\left(\frac{A_0L^2}{K}\right)L^3}{\alpha\nu} \tag{9}$$

2.2. Partitioning Wall

When the thickness of the partitioning wall is finite, the wall constitutes a third thermally-active layer in addition to the two main convection layers separated by its existence. The two-dimensional diffusion equation applies here

$$\frac{\partial^2\phi}{\partial r^2}+\frac{1}{r}\frac{\partial\phi}{\partial r}+\frac{1}{r^2}\frac{\partial^2\phi}{\partial\theta^2}=0 \tag{10}$$

2.3. Boundary Conditions

Because of symmetry of the flow system, the half region ($0°\leq\theta\leq180°$) only will be considered. The imposed boundary conditions are at $r=R$, r_i and r_0,

$$\Psi=0$$
$$\frac{\partial\Psi}{\partial r}=0$$
$$\frac{\partial\Psi}{\partial\theta}=0$$
$$\zeta_w=\frac{2(\Psi_w-\Psi_{w\pm1})}{(\Delta r)^2}$$

at $r=r_0$, $\phi=0$ (11)

and at $\theta=0$ and π,

$$\Psi=0$$
$$\frac{\partial\Psi}{\partial r}=0$$
$$\frac{\partial\phi}{\partial\theta}=0$$
$$\zeta=0$$

Whether the wall thickness is finite or negligible, energy is conserved locally and there is no abrupt change in temperature or heat flux at the fluid-solid or fluid-fluid interface. Thus, the thermal boundary condition at the interfaces $r=R$ and $r=r_i$ is

$\phi_1=\phi_2$ (Dirichlet type)

or (12)

$$K_1\frac{\partial\phi}{\partial r}\Big|_1=K_2\frac{\partial\phi}{\partial r}\Big|_2 \text{(Neumann type)}$$

where subscripts 1 and 2 indicate the two materials in contact at the interface.

3. Finite Difference Method

Near the wall, the gradient of the flow characteristics is high. In this study, denser grid is provided near the wall than in other regions by an abrupt change in grid size, whose ratio is kept less than 2 for accuracy. The mesh system is shown in Fig. 1. At the center, Cartesian coordinates are patched to the cylindrical coordinates to remove the coordinate singularity, as shown in the left hand side of Fig. 1. For variable mesh system, the first and the second order derivatives can be discretized as

$$\frac{\partial\Gamma}{\partial\lambda}=\frac{\Gamma_{i+1}-\Gamma_{i-1}}{\Delta\lambda_1+\Delta\lambda_2} \quad (13)$$

$$\frac{\partial^2\Gamma}{\partial\lambda^2}=\frac{\Gamma_{i+1}-(1+S^2)\Gamma_i+S^2\Gamma_{i-1}}{(\Delta\lambda_2)^2} \quad (14)$$

where $S=\Delta\lambda_2/\Delta\lambda_1$, and Γ and λ represent the dependent and independent variables, respectively. Each of the governing equations is then discretized into the following general form

$$\Gamma_{i,j}=A_{i,j}\,\Gamma_{i+1,j}+B_{i,j}\,\Gamma_{i-1,j}+C_{i,j}\,\Gamma_{i,j+1}+D_{i,j}\,\Gamma_{i,j-1}+E_{i,j} \quad (15)$$

The successive overrelaxation(*S.O.R.*) technique is adopted to solve the above penta-diagonal matrix iteratively.

In order to eliminate skewness of the point S.O.R., the sweep direction is chosen to be opposite in consecutive iteration loop for each variable, reference(9). A careful choice of relaxation factors was crucial to the convergence.

The equations were solved in the following steps.

(1) Assume the initial and boundary conditions
(2) Solve the cylindrical core region with a Neumann type thermal boundary condition at the interface $r=R$.
(3) Solve the annular region with a Dirichlet type thermal boundary condition at the interface $r=r_i$.
(4) Solve the conduction region by the boundary integral equation method which is given in the references (10) and (11), with the boundary conditions of Dirichlet type at $r=R$ and of Neumann type at $r=r_i$. These boundary conditions are copied from the flow properties of the adjoining flow at the interface using Eq.(12).

Then we iterate through steps 2, 3 and 4 until convergence is achieved. The boundary conditions necessary in steps 2 and 3 are copied from the conduction region by using Eq.(12), again. When the wall thickness is negligible, step 4 is omitted and the boundary conditions for steps 2 and 3 are obtained by transcribing the flow properties from the adjoing region, Eq.(12).

4. Results and Discussion

4.1. Normalization

In order to compare the present results with the corresponding states of conduction, the nondimensional temperature and its gradient are respectively normalized by those of the corresponding conduction problem. In the corresponding problem, the fluid in the annular region is frozen with time, its thermal conductivity being equal to that of the fluid under consideration. The inner boundary $r=r_i$ and the outer boundary $r=r_0$ are isotherms of different values: The temperatures at $r=r_0$ is fixed by $\phi=0$ and at $r=r_i$ a constant temperature is assigned such that the total heat flux is equal to that of the current problem for each Rayleigh number.

The temperature, its gradient and total heat flux of the corresponding conduction problem are, in nondimensional form,

$$\phi=\phi_{icd}\frac{\ln(r_0/r)}{\ln(r_0/r_i)} \tag{16}$$

$$\left.\frac{\partial\phi}{\partial r}\right|_{cd}=\frac{-\phi_{icd}}{\ln(r_0/r_i)}\cdot\frac{1}{r} \tag{17}$$

$$Q=\frac{2\pi\phi_{icd}}{\ln(r_0/r_i)} \tag{18}$$

where ϕ_{icd} is the temperature at the inner boundary $r=r_i$ in the conduction problem, and Q is the heat flux scaled by the quanity A_0L^2. The dimensionless total heat flux generated in the cylindrical core region is

$$Q=\pi R^2 \tag{19}$$

By equating Eq.(18) and Eq.(19),

$$\phi_{icd}=\frac{R^2}{2}\ln(r_0/r_i) \tag{20}$$

The normalized temperature and its gradient are, respectively,

$$\bar{\phi}=\frac{\phi}{\phi_{icd}} \tag{21}$$

$$\frac{\partial\bar{\phi}}{\partial r}=\frac{\frac{\partial\phi}{\partial r}}{\left.\frac{\partial\phi}{\partial r}\right|_{cd}} \tag{22}$$

Let $\bar{\phi}_{iav}$ represent the average value of $\bar{\phi}$ along the inner boundary, then the relation between $\bar{\phi}_{iav}$ and Q is in a simplified form

$$Q=\frac{\bar{\phi}_{iav}}{R_{th}} \tag{23}$$

where R_{th} is the thermal resistance of the annular gap. As Q in dimensionless form is a constant from Eq(19), $\bar{\phi}_{iav}$ linearly depends on R_{th}, that is, $\bar{\phi}_{iav}$ represents a measure of thermal resistance of the annular gap. The convective effect on the heat transfer through the gap is verified by the average normalized temperature. Fig. 2 represents the local variation of $\bar{\phi}$, in terms of the Rayleigh number, along the inner

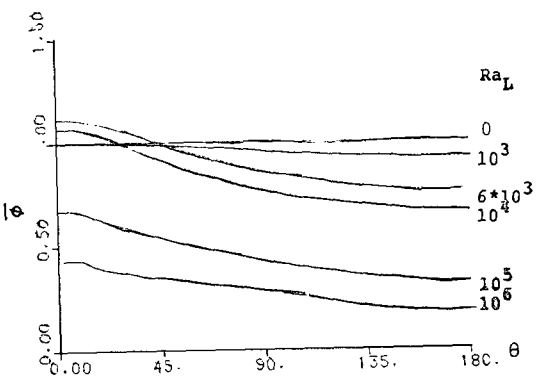

Fig. 2 Circumferential temperature distributions on the inner cylinder ($r=r_i$) with negligible wall thcikness

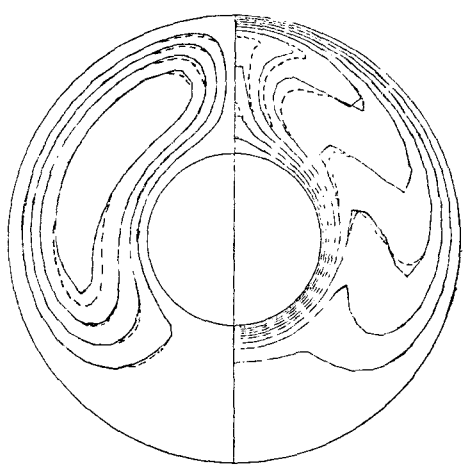

Fig. 3 Concentric annulus with isothermal boundaries: —present, ···Keuhn and Goldstein[1].

cylinder wall with negligible thickness. We can read that the normalized temperature decreases in average with the increase of the Ra_L, reflecting the fact that effect of convection reduces the thermal resistance in the gap.

To validate the current method, a test calculaton was carried out for a pure annular problem. Fig. 3 compares the result of the present method with that of Kuehn and Goldstein[1] for $Ra_L=10^5$, $Pr=0.7$ and diameter ratio 2.6, when the inner and outer boundaries of the annulus are isotherms. The two results compare very well in the boundary layers, although some minor discrepancy is developed in the central region of the annulus where grid is relatively coarse.

4.2. Effect of the Wall Thickness

When the thermal conductivity of the partitioning wall is much higher than that of the surrounding fluids, and the wall is quite thick, the condition at $r=r_i$ becomes nearly isothermal. As mentioned earlier, the annuli with isothermal boundaries have been investigated a lot.

In the present study, we took the wall thickness as one twentieth and a hundredth of the annular gap and compared the result with that of the negligible wall thickness.

Fig. 4 shows the three cases, where the wall thickness is taken as zero, $L/20$ and $L/100$, respectively. When the thermal conductivity of the wall is very high, the temperature gradient in the fluid at the interface must be also very high by the second equation of Eq.(12). Then, it requires an excessive degree of grid clustering near the wall for proper computational accuracy and stability. Due to the limited computer resources, however, we took the wall conductivity as 15 to 50 times that of the fluid. Nevertheless, for this relatively low values of conductivity we were able to draw some meaningful conclusion in a limited scope on the effect of the wall

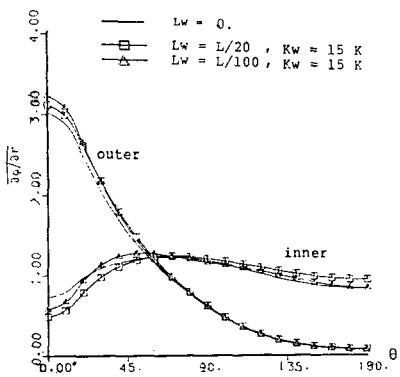

Fig. 4(a) Temperature Gradient on $r=r_i$(inner wall) and $r=r_0$ (outer wall) of the annulus for fixed wall conductivity

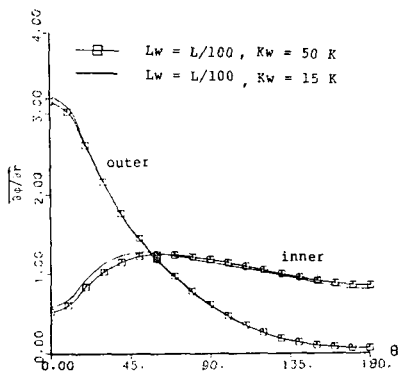

Fig. 4(b) Temperature Gradient on $r=r_i$(inner wall) and $r=r_0$ (outer wall) of the annulus for fixed wall thickness

thickness. Fig. 4 (a) shows the gradient of the normalized temperature along the annular boundaries for different wall thickness, with $Ra_L=1.0\times10^5$, $Pr=0.7$, diameter ratio $r_0/r_i=2.6$ and wall conductivity $K_W=15K$. The results do not deviate much from each other. Fig.4(b) shows the cases of two different wall conductivities $K_W=15K$ and $50K$. Almost no difference is revealed between the two. As a result, when the partitioning wall is thin and its thermal conductivity is relatively not so high in comparison with that of the surrounding fluid, the effect of the wall thickness can be safely neglected in engineering sense. We now further investigate the effect of the other parameters in the rema-

ining sections assuming negligible wall thickness.

4.3. Effect of the Rayleigh Number

The effect of Rayleigh number, in the parameter range studied, turns out much more distinguished than the others.

Around $Ra_L=10^3$, transition from the conduction mode begins to occur. In Fig. 5(c), the temperature distribution in the radial direction does not deviate much from that of the pure conduction given by Eq.(16). The isotherms in Fig. 6(a) shows that they are circles with slight eccentricity in both of the cylindrical core and the annular gap. This has been called "Pseudo-Conductive regime" by Grigull and Hauf[12], since the overall heat transfer characteristics are essentially those of the pure conduction.

As the Rayleigh number increases, the "pseudo-conductive mode is changed. The isotherms are deformed more and more in the upper region of the annulus and in the recirculating region, suggesting growing intensity of the convection. The thermal boundary layer develops accordingly in the annular gap near the lower portion of the cylinder $r=r_i$ and near the upper portion of the outer boundary $r=r_0$. The development procedure of this thermal convection with the increasing Rayleigh number is sequentially shown in Figs. 5~11..

It is interesting to note the change in the radial temperature distribution for different Rayleigh numbers. The temperature curves are spread apart for different θ up to $Ra_L=10^4$, making the curves fatter near the middle of the annular gap with increasing Rayleigh number,as observed in the $\bar{\phi}$ plots in Figs. 5~8. This increased variation of the normalized temperature $\bar{\phi}$ is due to the rapid development of the convection layers, which induces lower temperature toward the relatively inert bottom region ($\theta=180°$) and higher temperature toward the buoyant upper

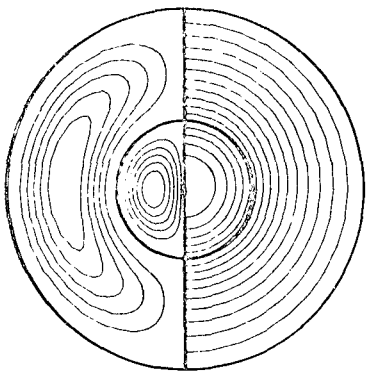

(a) Streamlines and isotherms

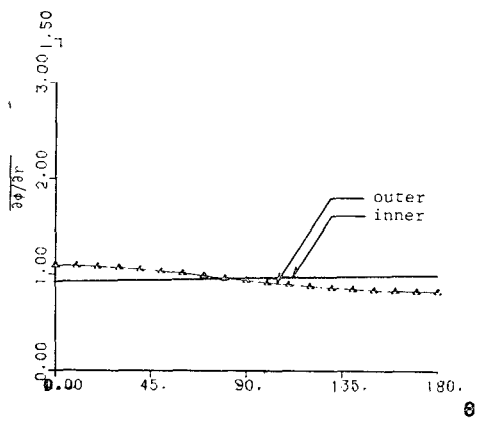

(b) Temperature gradient

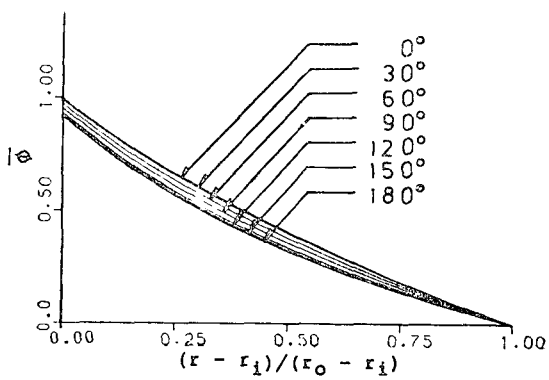

(c) Radial temperature distribution

Fig. 5 $Ra_L=1.0\times10^3$, $Pr=0.7$, $r_0/r_i=2.6$

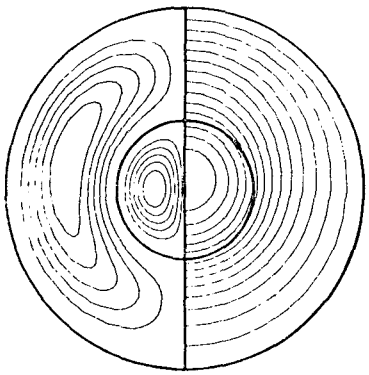

(a) Streamlines and isotherms

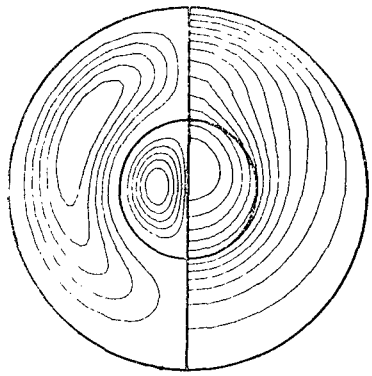

(a) Streamlines and isotherms

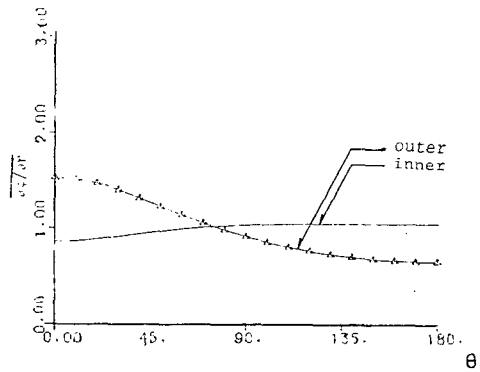

(b) Temperature gradient

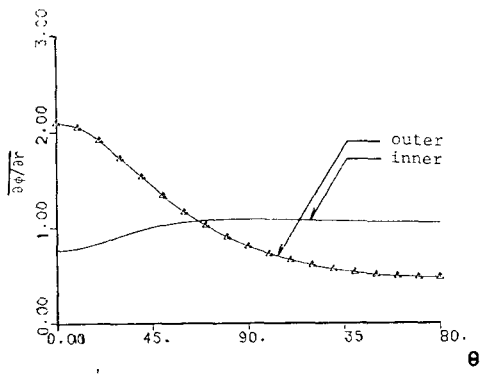

(b) Temperature gradient

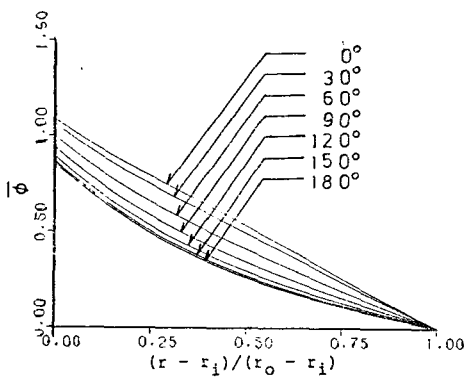

(c) Radial temperature distribution

Fig. 6 $Ra_L=3.0\times10^3$, $Pr=0.7$, $r_o/r_i=2.6$

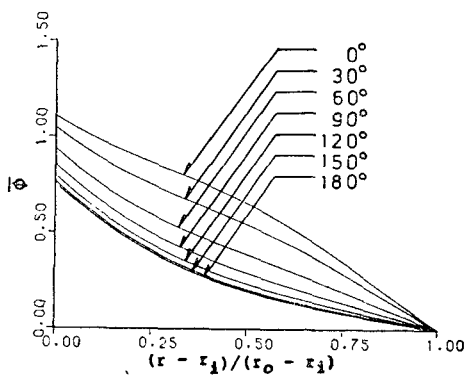

(c) Radial temperature distribution

Fig. 7 $Ra_L=6.0\times10^3$, $Pr=0.7$, $r_o/r_i=2.6$

region ($\theta=0°$) of the annulus. For $Ra_L>10^4$, Figs. 9~11, the normalized temperature becomes widely flat in the gap except near the boundaries, and its maximum values at the partitioning wall $r=r_i$ are much lowered. This is due to the fact that as Ra_L ($>10^4$) increases, the recirculating current becomes stronger, causing the thermal resistance of the annular gap to decrease significantly: recall the earlier discussion associated with Fig. 2.

Irrespective of the Rayleigh numbers, the normalized total heat flux remains a constant for a given core radius R, see Eq.(19). Hence, the local temperature gradient presented in the second plot of Figs. 5~14 indicates the degree of contribution to the total heat transfer from the local position of the boundaries. At $Ra_L=10^3$ in Fig. 5, the flow is in the so-called pseudo-conductive regime, so the temperature gradients are almost equal to unity on both of the boundaries. The mode of heat transfer on the outer boundary $r=r_0$ depends on Ra_L more than it does on the inner boundary $r=r_i$. As Ra_L increases, the strong recirculating current causes the gradient on the outer boundary to experience large variation; on the inner boundary, relatively smaller variation is made around the value of unity since the cylinder $r=r_i$ is amid the overall convection and the boundary layer is relatively well developed throughout along its surface.

It is worthwhile to note some characteristic difference in the radial temperature gradient between the present problem and the case of concentric annulus with isothermal boundaries[1]. In the latter case, the temperature gradient along $r=r_i$ decreases monotonously as the flow moves from the bottom stagnation point($\theta=180°$) to the top($\theta=0°$). In the present problem, the curves of temperature gradient on the inner boundary $r=r_i$ develop a plateau of peak values with the increasing Rayleigh numbers, see the

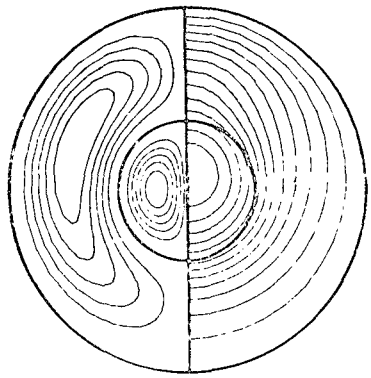

(a) Streamlines and isotherms

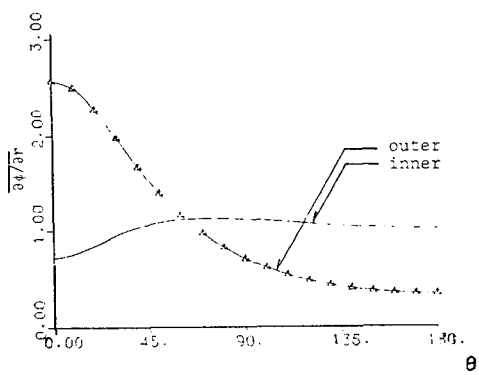

(b) Temperature gradient

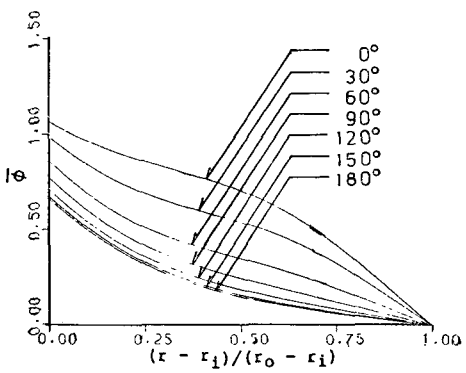

(c) Radial temperature distribution

Fig. 8 $Ra_L=6.0\times10^4$, $Pr=0.7$, $r_0/r_i=2.6$

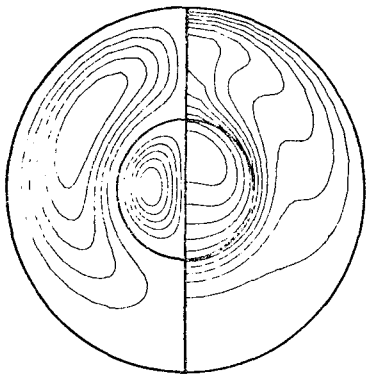

(a) Streamlines and isotherms

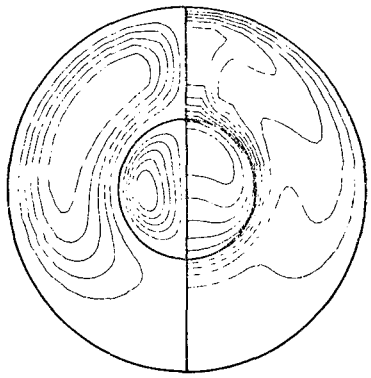

(a) Streamlines and isotherms

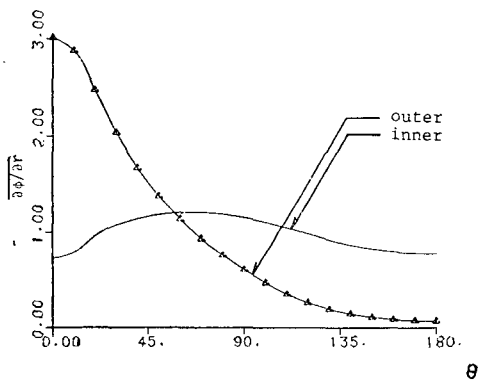

(b) Temperature gradient

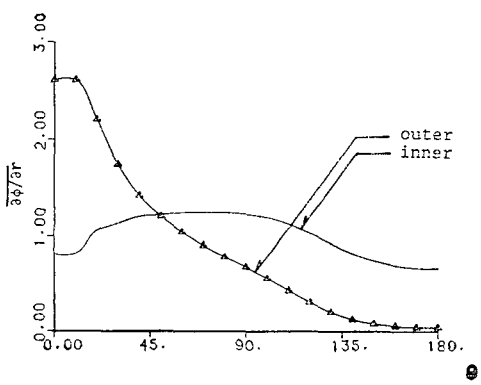

(b) Temperature gradient

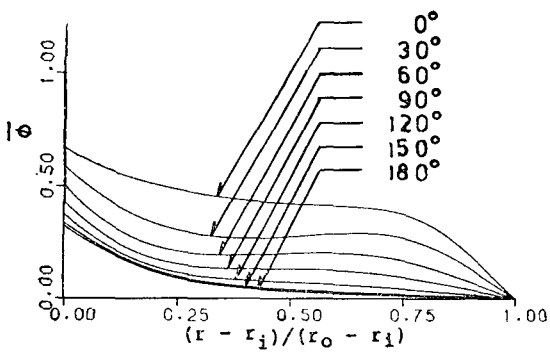

(c) Radial temperature distribution

Fig. 9 $Ra_L=1.0\times10^5$, $Pr=0.7$, $r_o/r_i=2.6$

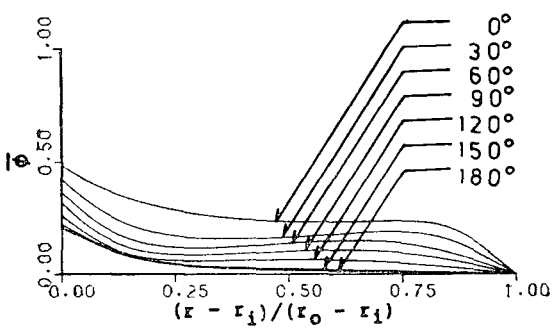

(c) Radial temperature distribution

Fig. 10 $Ra_L=5.0\times10^5$, $Pr=0.7$, $r_o/r_i=2.6$

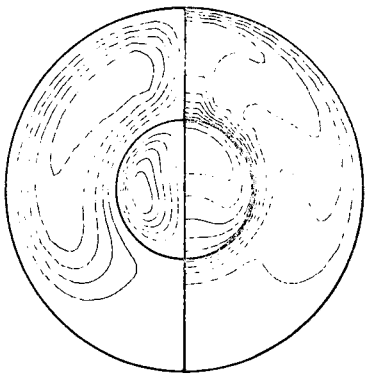

(a) Streamlines and isotherms

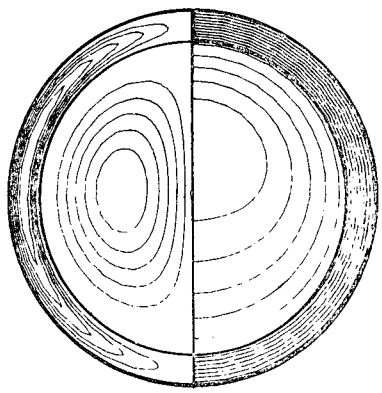

(a) Streamlines and isotherms

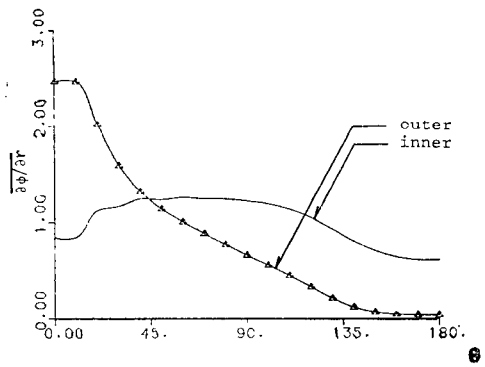

(b) Temperature gradient

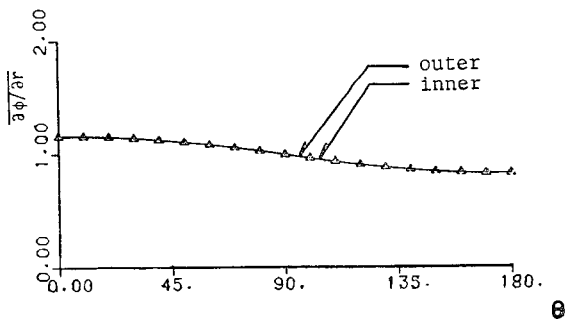

(b) Temperature gradient

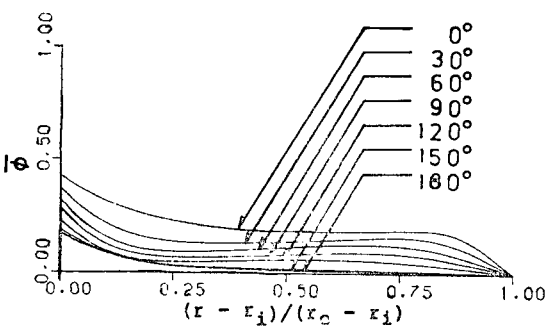

(c) Radial temperature distribution

Fig. 11 $Ra_L=1.0\times10^6$, $Pr=0.7$, $r_0/r_i=2.6$

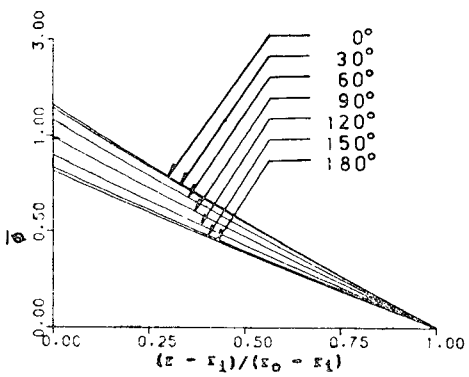

(c) Radial temperature distribution

Fig. 12 $Ra_{Di}=1.0\times10^5$, $Pr=0.7$, $r_0/r_i=1.2$

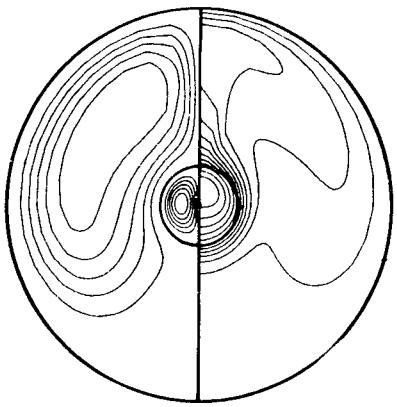

(a) Streamlines and isotherms

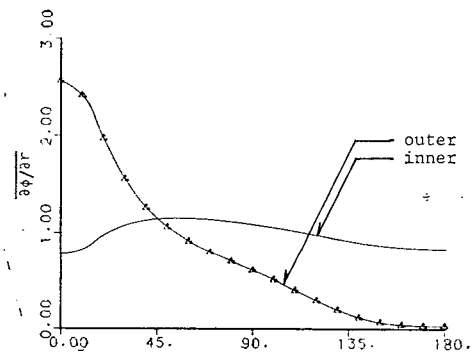

(b) Temperature gradient

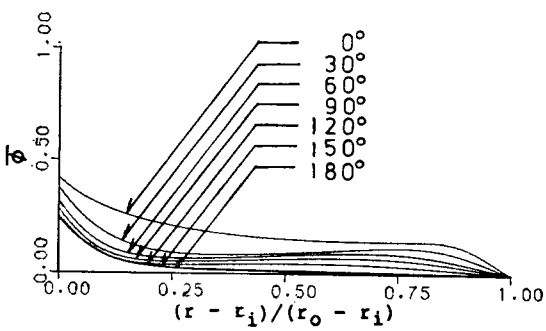

(c) Radial temperature distributon

Fig. 13 $Ra_{Di}=1.0\times10^5$, $Pr=0.7$, $r_o/r_i=5.0$

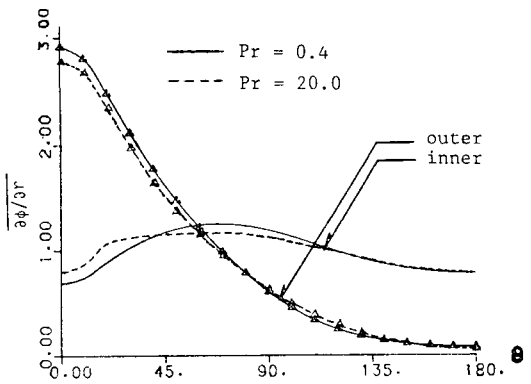

Fig. 14 Radial temperature gradient for different Prandtl numbers

second plots in Figs. 5~11. This phenomenon can be interpreted as the result of interactive convection from the heat-generating cylindrical core region. The thin boundary layer developed along inside surface of the partitioning wall in the core region ($r=R$), presents a large radial gradient of temperature, for example, in the region $30°\leq\theta\leq100°$ in Fig. 11(a). The characteristic plateau in Fig. 11(b) is caused by this interactive boundary layer.

The temperature inversion phenomenon, by which the fluid near the cold surface is warmer than the fluid near the hot surface in the annular region, is observed for $Ra_L>1.0\times10^5$(Figs. 9~11). It is due to the influence of strong recirculating current for high Rayleigh numbers. For the low Rayleigh number flows, Figs. 5~8, the radial temperature curves develop inflection points suggesting growing effect of the convection, which will eventually progress toward the temperature inversion at higher Rayleigh number.

4.4. Effect of the Diameter Ratio

As the diameter ratio is taken smaller($r_o/r_i=1.2$) for a fixed Rayleigh number $Ra_{Di}=1.0\times10^5$ and Prandtl number $Pr=0.7$, Fig. 12, where Ra_{Di} is based on the diameter of the in-

ner cylinder, the effect of the conjugate convection from the cylindrical core is weakened while the conduction effect becomes dominant in the annular region. The straight temperature curves, the coincident radial temperature gradients for the boundaries $r=r_0$ and $r=r_i$, and the nearly concentric isotherms all support such a claim. The heat flux occurs mainly in the radial direction, suggesting pseudo-conduction heat transfer. As we take $r_0/r_i=5.0$ for the same Ra_{Di} and Pr, Fig. 13, we observe that the recirculating flow is increased in scale but slowed in velocity and the inert region at the bottom of the annular gap is increased. It causes the temperature to become flatter in this region. In the cylindrical core, the viscous effect is diffused throughout in the relatively narrowed region. Thus, boundary layer on the inside surface of the boundary $r=R$ is not as well developed as the case of $r_0/r_i=2.6$, the effect of which is represented by the smoother temperature gradient on the boundary $r=r_i$ in the annular gap, Fig. 13(b).

4.5. Effect of the Prandtl Number

The effect of the Prandtl number is the least among the parameters considered, In Fig. 14, the temperature gradient is compared between $Pr=0.4$ and $Pr=20.0$, for fixed $Ra_L=1.0\times10^5$ and $r_0/r_i=2.6$. The variation is very small. This relative indifference was even stronger in the comparison of the local temperature distributions, the streamlines and the isotherms, which are not shown here.

5. Conclusion

The conjugate natural convection heat transfer in a horizontal system of thermally active composite layers has been analyzed by the finite difference method. The development procedure of the convection layers with the Rayleigh number in the annulus and in the core region is sequentially presented using the graphics of the streamlines and isotherms, and the temperature curves. It has been argued in a quantitative manner that the thermal resistance in the annular gap decreases for higher Rayleigh number due to the increased convection activity.

The interactive boundary layer developed along the wall in the core region makes the distribution of the radial temperature gradient along the partitioning wall characteristically different from that of the pure concentric annuli problems. The interaction between the annulus and the core region undergoes fundamental change for different ratios of the outer and inner cylinder diameters, depending upon the relative degree of diffusion of the viscous effect in either of the composite layers. Among the many parameters investigated, the parameters of the partitioning wall and the Prandtl number gave least influence in the parameter range studied.

References

(1) T.H. Kuehn and R.J. Goldstein, "An Experimental and Theoretical Study of Natural Convection in the Annulus Between Horizontal Concentric Cylinders," J. Fluid Mech. Vol. 72, Part 4, pp. 695~719, 1976

(2) B. Farouk and S.I. Guceri, "Laminar and Turbulent Natural Convection in the Annulus Between Horizontal Concentric Cylinders," ASME J. Heat Transfer, Vol. 104, No. 4, pp. 631~636, 1982

(3) C.H. Cho, K.S. Chang and K.H. Park, "Numerical Simulation of Natural Convection in Concentric and Eccentric Horizontal Cylindrical Annuli", ASME J. Heat Transfer, Vol. 104, No. 4, pp. 624~630, 1982

(4) J.Huetz and J.P. Petit, "Natural and Mixed Convection in Concentric Annular Space-Experimental and Theoretical Results for Liquid Metals", 5th

Int. Heat Transfer Conf. Tokyo, Vol. 3, pp. 169~172, 1974

(5) E. Van De Sande and J.G. Hamer, "Steady and Transient Natural Convection in Enclosures Between Horizontal Circular Cylinders (Constant Heat Flux)", Int. J. Heat Mass transfer, Vol. 22, No. 3, pp. 361~370, 1979

(6) Z. Rotem, "Conjugate free Convection from Horizontal Conducting Circular Cylinders," Int. J. Heat Mass Transfer, Vol. 15, No. 8, pp. 1679~1693, 1972

(7) R.J Kee, C.S. Landram and J.C. Miles, "Natural Convection of a Heat Generating Fluid Within Closed Vertical Cylinders and Spheres," ASME J. Heat Transfer Vol. 98, No. 1, pp. 55~61, 1976

(8) D.R. Jones, "Convective Effects in Enclosed Exothermically Reacting Gases", Int. J. Heat Mass Transfer, Vol. 17, No. 1, pp. 11~21, 1974

(9) P.J. Roache, *Computational Fluid Dynamics*, Hermosa Pub. 1972

(10) Y.P. Chang, C.S. Kang and D.J. Chen, "The use of Fundamental Green's Functions for the Solution of Problem of Heat Conduction in Anisotropic Media", Int. J. Heat Mass Transfer, Vol. 16, No. 10, pp. 1905~1918, 1973

(11) M.S. Khader and M.C. Hanna, "An Iterative Boundary Integral Numerical Solution for General Steady Heat Conduction Problems", ASME J. Heat Transfer, Vol. 103, No. 1, pp. 26~31, 1981

(12) U. Grigull and W. Hauf, "Natural Convection in Horizontal Cylindrical Annui", 3rd Int. Heat Transfer Conf., Chicago, pp. 182~195, 1966